RESEARCH ARTICLE | APRIL 07 2023

Oil–water two-phase flow-induced vibration of a cylindrical cyclone with vortex finder

Chen Hu (陈虎); Liu Shuo (刘硕) (iD); Zhang Jian (张健) ✉ (iD); Xu Jing-Yu (许晶禹) (iD)

Check for updates

View Online   Export Citation

08 April 2024 03:28:50

AIP Publishing

Oil–water two-phase flow-induced vibration of a cylindrical cyclone with vortex finder

View Online   Export Citation   CrossMark

Hu Chen (陈虎),[1,2] Shuo Liu (刘硕),[1,2] Jian Zhang (张健),[1,2,a] and Jing-Yu Xu (许晶禹)[1,2]

AFFILIATIONS

[1]School of Engineering Sciences, University of Chinese Academy of Sciences, Beijing 100049, China
[2]Institute of Mechanics, Chinese Academy of Sciences, Beijing 100190, China

[a]Author to whom correspondence should be addressed: zhangjian@imech.ac.cn

ABSTRACT

Cylindrical cyclones play an important role in oil–water separation and sewage treatment in the petroleum industry. Here, we describe the characteristics of vibration induced by a two-phase rotational flow in a cylindrical cyclone. The cyclone operating parameters together with a dimensional analysis and multiphase flow numerical simulation were used to understand the flow field characteristics. The frequency and amplitude of pressure fluctuation were obtained by measuring pressure changes at points on the axis of the device. It shows that the pressure in a cylindrical cyclone varies periodically during separation and that fluctuation frequency and amplitude are related to the inlet velocity and flow split ratio. The effect of the overflow split ratio on the pressure fluctuation frequency is negligible, but increasing the overflow split ratio will cause greater fluctuation of the flow. For a cylindrical cyclone, the pressure fluctuation frequency can be calculated from the inlet velocity. Adjusting the inlet velocity and the overflow split ratio changes the mechanical response of the structure. The results of a modal analysis show that the structural vibration response is consistent with the response state of the lowest point of the internal central-vortex pressure and that both are in approximate circular motion. Furthermore, the frequency of pressure fluctuation induced by the flow is close to the intrinsic frequency of the structure with a single bottom constraint, which can cause unwanted resonance easily. Therefore, an appropriately added constraint on a cylindrical cyclone should be taken into consideration to avoid the resonance frequency.

I. INTRODUCTION

Oil–water mixtures are extracted by offshore oil wells, and oil–water mixtures with high water content exist on many offshore oil production platforms.[1,2] Efficient oil–water two-phase separation technology can greatly improve the economic benefits of oil exploration. As distinct from onshore oil exploration platforms, offshore platforms have a smaller operation space. So, it is important that the separation equipment is fabricated to be as small as possible. The hydrocyclone has attracted wide attention owing to its small size and high separation efficiency.[3,4]

The hydrocyclone uses the difference in density between oil and water for centrifugal separation.[5] There has been a lot of research works on classic hydrocyclones;[6,7] our research is focused on a more easily controlled cylindrical cyclone. Since Afanador[8] first proposed the concept of the cylindrical cyclone with tangential inlet in 1999, researchers have conducted theoretical analysis, experiment, and numerical simulation on various cylindrical cyclones to better understand the separation mechanism. Experiments and numerical simulations showed that

cylindrical cyclones are very effective for separating oil and water phases.[9,10] Mathiravedu et al.[11] studied the characteristics of oil–water two-phase separation by an experimental method and proposed a linear control system comprising a liquid–liquid cylindrical cyclone with water content at the down-outlet as the control variable, so as to keep clear water from the down-outlet. Liu et al.[12] carried out oil–water two-phase separation research in a liquid–liquid cylindrical cyclone by experimental and numerical simulation methods. They studied the effects of overflow split ratio and inlet flow rate on separation efficiency and showed that there is an optimum overflow split ratio and an optimum inlet flow rate range for oil–water two-phase separation with a cylindrical cyclone. Shi et al.[13] studied the effect of design parameters of a vortex finder on oil–water two-phase separation performance of a liquid–liquid cylindrical cyclone. They showed that under certain operating conditions, there are optimum design parameters for the vortex finder in a cylindrical cyclone to achieve the best oil–water separation effect.

The internal flow and the pressure fluctuations inside pipes can generate system vibration. This flow-induced vibration can destroy the

stability of the structure itself, which is a common problem in a pipeline system.[14–16] Pettigrew *et al.*[17] described how a two-phase flow-induced vibration is more complex than that caused by a single-phase flow. Kabiri-Samani *et al.*[15] studied the flow-induced vibration of a gas–water two-phase flow in horizontal and inclined pipe conditions. They showed that the gas–water mixture during the rapid filling of surcharging can cause a tremendous pressure surge and may even eventually cause the collapse of the pipe. Grimble and Agarwal[18] and Grimble *et al.*[19] measured the radiated sound spectra of a cyclone to research cyclone hum. The adventitious flow in the vortex core was investigated using a local linear-stability analysis, which revealed that significant oscillation occurred in the flow field due to the coupling of strong swirling flow field and the vortex finder; the instability of this flow was a source of acoustic noise.

II. NUMERICAL METHODS AND MODELING

Considering previous research,[10,12] we designed a cylindrical cyclone with vortex finder, which consists of five parts: tangential inlet, main cylinder, vortex finder, down-outlet, and up-outlet. A schematic diagram of the cylindrical cyclone with vortex finder is shown in Fig. 1. All structural parameters are listed in Table I.

First, a dimensional analysis was used to determine the parameters that affect the oil–water two-phase flow-induced vibration of the cylindrical cyclone with vortex finder. The relevant parameters and their dimensions are listed in Table II.

The frequency of pressure fluctuation can be expressed as[10]

$$f = \varphi(D_{in}, \gamma, D_m, D_{over}, D_{under}, L_m, L_f, v_{inlet}, \lambda_{over}, \Delta\rho). \quad (1)$$

The D_{in}, v_{inlet}, and $\Delta\rho$ were selected as units, so that Eq. (1) can be written in dimensionless form as follows:
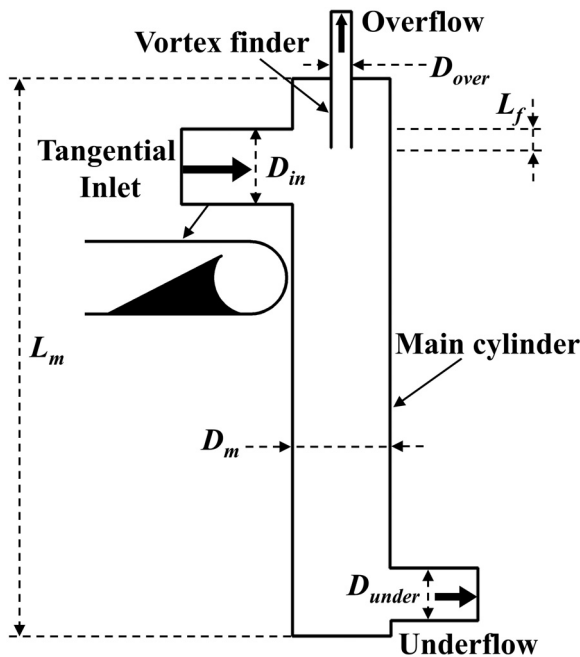

FIG. 1. Schematic diagram of the cylindrical cyclone with vortex finder.

TABLE I. Structural parameters of the cylindrical cyclone with vortex finder.

Parameter	Value (mm)	Parameter	Value (mm)
D_{over}	25	L_m	1250
L_f	150	D_m	100
D_{in}	100	D_{under}	80

$$\frac{D_{in}f}{v_{inlet}} = \varphi\left(\gamma, \frac{D_m}{D_{in}}, \frac{D_{over}}{D_{in}}, \frac{D_{under}}{D_{in}}, \frac{L_m}{D_{in}}, \frac{L_f}{D_{in}}, \lambda_{over}\right). \quad (2)$$

Shi *et al.*[13] showed that the diameter of the inlet pipe should always equal that of the main cylinder and that the diameter of the underflow pipe has little effect on the flow or any subsequent separation. The tangential inlet contraction ratio and inlet flow rate can be combined to form an influencing factor. In addition, Ghodrat *et al.*[20] showed that the effect of the vortex finder length on separation is much less significant than the effect of diameter. The simplified influencing factors on the pressure fluctuation frequency are the diameter of the inlet pipe, the diameter of the overflow pipe, the length of the main cylindrical pipe, the inlet velocity, and the overflow split ratio. Therefore, Eq. (2) can be simplified as

$$\frac{D_{in}f}{v_{inlet}} = \varphi\left(\frac{D_{over}}{D_{in}}, \frac{L_m}{D_{in}}, \lambda_{over}\right). \quad (3)$$

As we can see from Eq. (3), the oil–water two-phase flow-induced vibration of the cylindrical cyclone with vortex finder is mainly affected by the diameter of the inlet pipe, the diameter of the overflow pipe, the length of the cylinder, the inlet velocity, and the overflow split ratio. Cylindrical cyclones with fixed structures are mainly affected by the inlet velocity and the overflow split ratio.[12] The relationship between these effects can be determined by numerical simulation.[21]

Euler–Lagrange and Euler–Euler models were used to simulate two-phase flow.[22] When the Euler–Lagrange model was used to calculate a two-phase flow, one phase was described as continuous and the other as discrete. When the Euler–Euler method was used to calculate a two-phase flow, both phases were described as continuous.[23,24] For this work, both of two-fluid model and mixture model can be used to simulate oil–water two-phase flow in the cylinder cyclone with vortex finder.

TABLE II. The relevant parameters and dimensions of the cylindrical cyclone with vortex finder.

Parameter	Symbol	Dimension
Diameter of the inlet pipe	D_{in}	L
Contraction ratio of the tangential inlet	γ	1
Diameter of the main cylindrical pipe	D_m	L
Diameter of the overflow pipe	D_{over}	L
Diameter of the underflow pipe	D_{under}	L
Length of the main cylindrical pipe	L_m	L
Length of the vortex finder	L_f	L
Inlet velocity	v_{inlet}	LT^{-1}
Overflow split ratio	λ_{over}	1
Difference in density between oil and water	$\Delta\rho$	ML^{-3}

However, the mixture model was chosen in our numerical simulation work in order to save the calculation time. The mixture model regards the oil–water phases as a single mixed phase.[25] To solve the control equation, the mixture model ignores the interfacial effect between the two phases, introduces a slip velocity to describe the flow of the two phases, and the density and viscosity of the mixture are described by a linear weighted average. Then, the governing equation of the mixture is solved. The accuracy of the numerical simulation method was verified in our previous work.[26] It is sufficient for this work.

The continuity equation of the mixture is

$$\frac{\partial}{\partial \boldsymbol{t}}(\rho_m) + \nabla \cdot (\rho_m \boldsymbol{u_m}) = 0. \tag{4}$$

The momentum equation of the mixture is

$$\frac{\partial}{\partial t}(\rho_m \boldsymbol{u_m}) + \nabla \cdot (\rho_m \boldsymbol{u_m u_m}) = -\nabla P + \nabla \cdot \left[\mu_m\left(\nabla \boldsymbol{u_m} + \nabla \boldsymbol{u_m}^T\right)\right]$$
$$+ \rho_m \boldsymbol{g} + \boldsymbol{F} + \nabla \cdot \left(\sum_{k=1}^{n} \alpha_k \rho_k \boldsymbol{u_{dr,k} u_{dr,k}}\right), \tag{5}$$

where $\boldsymbol{F}$ is the other body force excluding gravity, and it is not considered in this work. ρ_m, μ_m, and $\boldsymbol{u_m}$ are the density, viscosity, and velocity of the mixture, respectively. The latter terms can be obtained by linear weighting as follows:[27]

$$\rho_m = \alpha_o \rho_o + (1 - \alpha_o)\rho_w, \tag{6}$$

$$\mu_m = \alpha_o \mu_o + (1 - \alpha_o)\mu_w, \tag{7}$$

$$\boldsymbol{u_m} = \frac{\alpha_o \rho_o \boldsymbol{u_o} + (1 - \alpha_o)\rho_w \boldsymbol{u_w}}{\rho_m}, \tag{8}$$

where $\boldsymbol{u}_{dr,k}$ is the drift velocity of phase k,

$$\boldsymbol{u}_{dr,k} = \boldsymbol{u_k} - \boldsymbol{u_m}. \tag{9}$$

As a key point of this study, the successful construction of the fluid–structure interaction model of the cylindrical cyclone was very important. The pressure of the fluid domain to the inner wall of the structure was applied, as the mechanism is shown in Fig. 2. The unidirectional fluid–solid coupling calculation method was chosen in this work in order to obtain the phenomenon of the flow-induced vibration of a cylindrical cyclone with vortex finder.

For solid domain calculations, the governing equations were obtained from Newton's second law,[28]

$$\rho_s \ddot{\boldsymbol{d}}_s = \nabla \cdot \boldsymbol{\sigma_s} + \boldsymbol{f_s}, \tag{10}$$

where ρ_s is the solid density, $\ddot{\boldsymbol{d}}_s$ is the local acceleration vector, $\boldsymbol{\sigma_s}$ is the Cauchy stress tensor, and $\boldsymbol{f_s}$ is the volume force vector. In addition, on the interface between the fluid domain and the solid domain (fluid–structure interaction surface), the stress of fluid and solid should be identical. The resultant force of the fluid distribution force was applied to the element nodes of structure according to the following equation:[29]

$$f(t) = \int \boldsymbol{h_s} \cdot \tau_f \, dA, \tag{11}$$

where h_s is the displacement of the structural node and dA is the area of infinitesimal element. Therefore, completely different grids can be
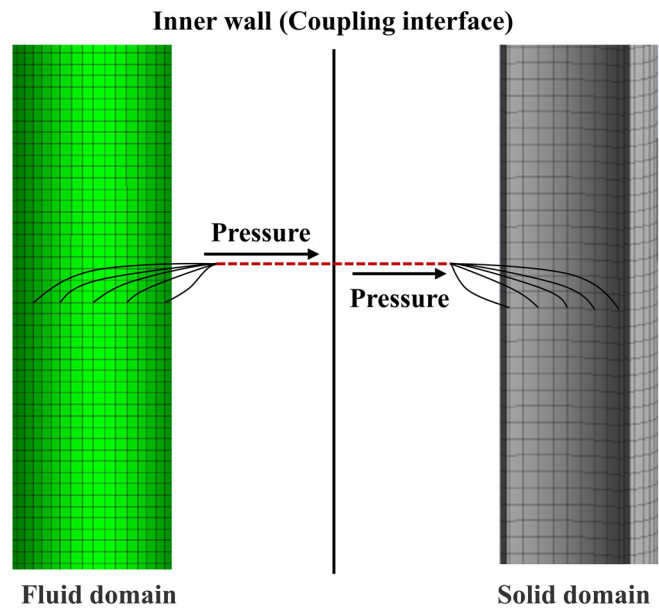

FIG. 2. Schematic diagram of unidirectional fluid–solid interaction mechanism.

used in fluid and structural models. The node positions of the two models are different at the fluid–structure interaction surface, but the time integration of the two models must be compatible.

For the modal analysis of the structure, the relationship between the natural frequency f_i and the vibration mode Φ_i of the cylindrical cyclone with vortex finder can be expressed as[30]

$$([K] - f_i^2[M])\{\phi_i\} = 0, \tag{12}$$

where $[K]$ is the stiffness matrix of the cylindrical cyclone, and $[M]$ is the mass matrix of the cylindrical cyclone.

The Integrated Computer Engineering and Manufacturing code for Computational Fluid Dynamics (ICEM CFD) software was used to create the computational grid over the surface and domain volume of the cylindrical cyclones. The resulting three-dimensional geometric model was divided into four parts: tangential inlet, main cylinder, up-outlet, and down-outlet. The O-blocking method was used to create the structural grid, as shown in Fig. 3. In order to test the influence of grid size on the simulation results, three different grid sizes were used for testing. The number of the three grids is about 1.23×10^6 (i.e., coarse-grid division scheme), 1.41×10^6 (i.e., medium-grid division scheme), and 1.62×10^6 (i.e., fine-grid division scheme). The static-pressure distribution on the cross section of the main cylinder for the three grid sizes is shown in Fig. 4. It shows that the coarse-grid scheme is different from the other two schemes and that the simulation results of the medium-grid scheme and the fine-grid scheme are not significantly different. Therefore, the subsequent numerical calculation adopted the medium-grid division scheme to ensure the calculation accuracy and efficiency. Approximately 1.41×10^6 elements were created for the model in this study.

The RNG k–ε turbulence model was used for numerical calculation,[31–33] and the SIMPLEC algorithm based on the finite-volume method was used for pressure–velocity coupling.[34,35] The primary
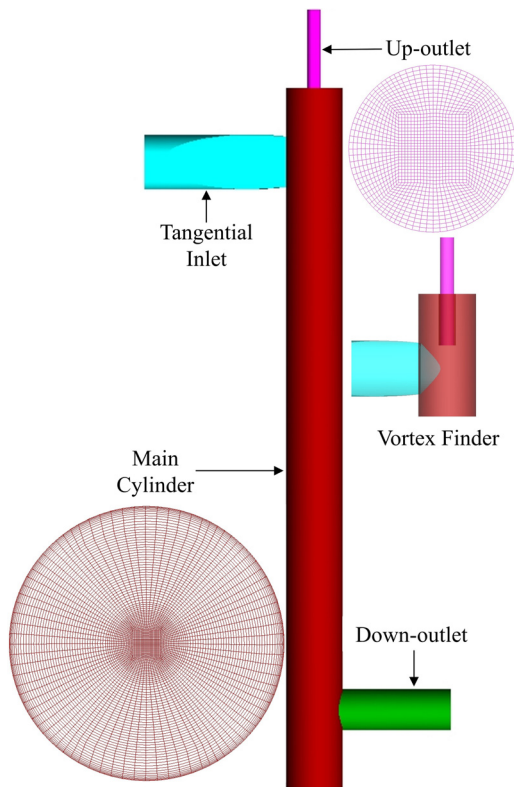
FIG. 3. Schematic diagram of grid partition for cylindrical cyclone.

TABLE III. Physical properties of oil and water in this study (T = 30 °C and P = 0.1 MPa).

	Density, kg/m³	Viscosity, mPa s	Surface tension, N/m
Oil	860	120	0.046
Water	998	1	0.071

velocity. The inlet oil droplet diameter and volume fraction are set to 0.1 mm and 0.1, respectively.[10] The outlets were set as the outflow boundary that can be used to control the flow split ratio expediently. The time step was set to 0.0005 s per calculation to better capture the change characteristics of the flow field.

The selection of calculation time length influences the subsequent spectrum analysis. Because the frequency resolution can be expressed as[36]

$$\Delta f = \frac{f_s}{N}, \tag{13}$$

the sampling time can be expressed as

$$t = \frac{N}{f_s}, \tag{14}$$

where f_s is the sampling frequency, and N is the number of sampling points.

From this, Δf can be written as

$$\Delta f = \frac{1}{t}. \tag{15}$$

It can be seen that frequency resolution is related to the sampling time. The longer the sampling time, the higher the frequency resolution accuracy and the more accurate the results. Therefore, three computing time lengths were considered to analyze the error caused by the calculation time lengths. The results of the spectrum analysis for the three calculation times are shown in Fig. 5. The results show that

phase in the flow was set as water, whereas the second phase was set as oil because the inlet oil volume fraction was less than 0.4 in our study. The physical property parameters of oil and water are listed in Table III. For the setting of boundary conditions, the inlet condition was used as a velocity inlet, which was convenient for controlling the inlet
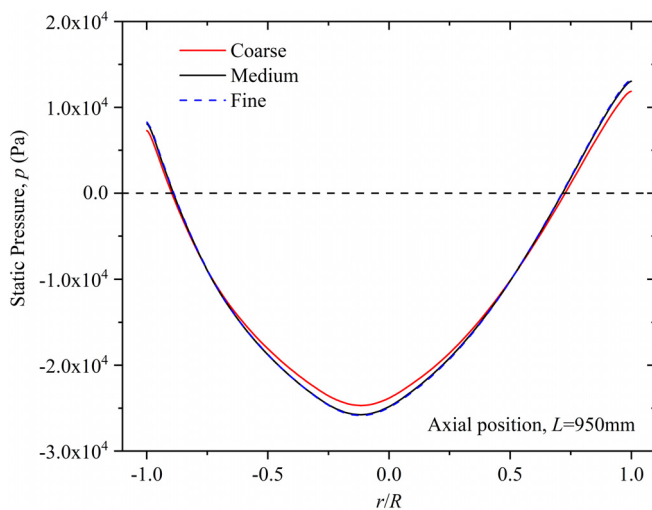

FIG. 4. The influence of grid generation on computational accuracy.
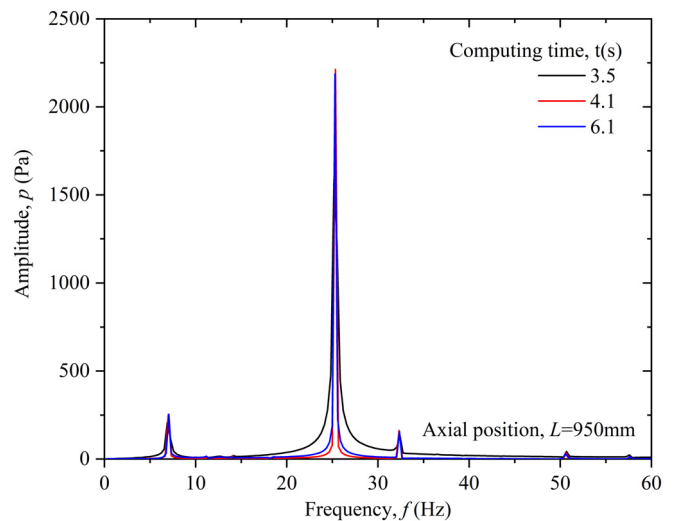

FIG. 5. Error analysis owing to calculation time.

the spectrum analysis has a small difference. For example, the difference between 25.17 Hz obtained in 3.5 s and 25.29 Hz obtained in 6 s is only 0.12 Hz. It shows a good calculation process.[37] Therefore, a further increase in computing time will not affect the calculated results, but will increase the calculation cost. To improve the calculation speed and ensure the calculation accuracy, the calculation time used in the subsequent analysis was 4.1 s.

III. TWO-PHASE FLOW FIELD IN THE CYLINDRICAL CYCLONE

The streamlines of the oil–water mixture during separation are shown in Fig. 6. It clearly shows that there is an upward internal swirl and a downward outer swirl in the cylindrical cyclone and that the light oil phase flows out from the up-outlet through the vortex finder and the heavy water phase flows out from the down-outlet, so separation is complete. However, the structural design of the one-sided tangential inlet introduces an asymmetric internal flow field to the device. The pressure distribution in the main cylinder is shown in Fig. 7. It can be seen that the pressure distribution along the radial direction is asymmetric. Our previous research deeply examined the separation mechanisms and influencing factors of the cylindrical cyclone, and our results showed that owing to the asymmetry of the internal flow field, the central vortex is of a spiral curved structure.[10] This asymmetric pressure distribution introduces pressure fluctuations and subsequent vibrations to the cylindrical cyclone during the separation process.

This work focuses on the study of the fluid–structure interaction characteristics of a cylindrical cyclone vortex finder used for oil–water two-phase separation. Consequently, there are two main research topics in this paper. The first is to simulate the unsteady flow in a
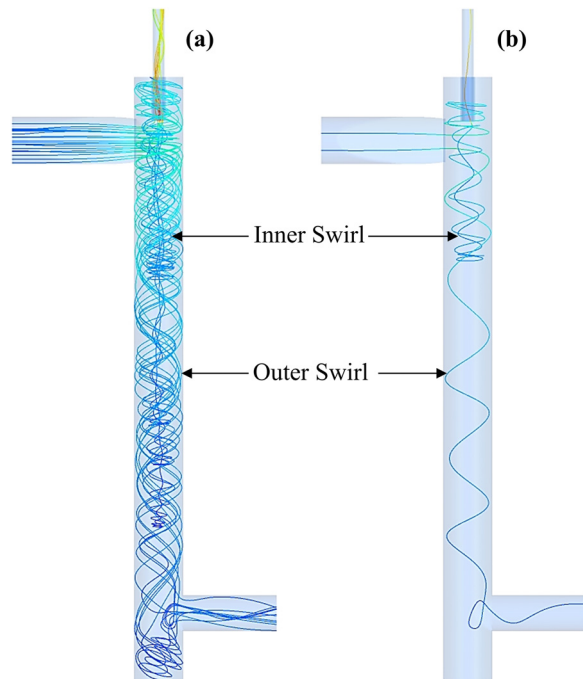

FIG. 6. Streamline diagram of the oil–water mixture in the cylindrical cyclone: (a) multiple streamlines and (b) two streamlines.
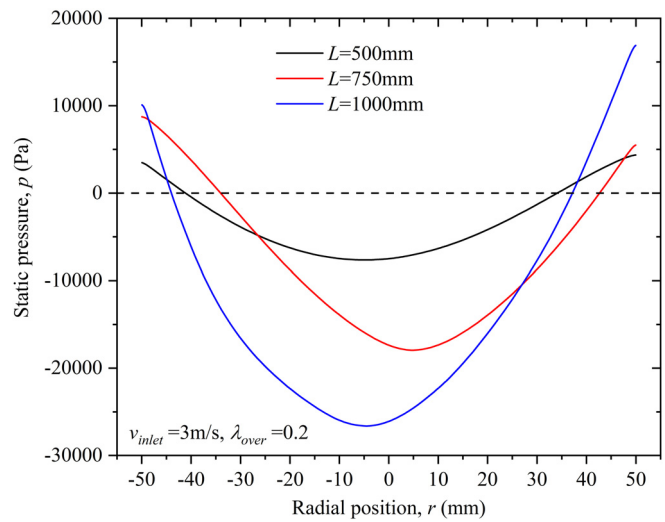

FIG. 7. Pressure distribution along the radial direction at different axial heights.

cylindrical cyclone and analyze its flow characteristics; the effects of inlet velocity and overflow split ratio on the flow characteristics are discussed. For the second, a fluid–structure interaction model is constructed to analyze the dynamics of the cylindrical cyclone structure and the change in structural mechanical properties caused by fluid flow therein is discussed.

IV. TWO-PHASE FLOW-INDUCED VIBRATION ANALYSIS

A. Flow field pressure fluctuation characteristics of the cylindrical cyclone

The analysis of the aforementioned central vortex shows that the fluid flow inside the cyclone is asymmetric owing to the structure of the one-sided inlet. The central vortex presents an asymmetric spiral bending structure; the bottom of the central eddy vibrates greatly, which results in a unsteady flow inside the cylindrical cyclone. In this section, the flow characteristics of the flow field inside the cylindrical cyclone under unsteady flow conditions are studied. The distribution of the cross-sectional pressure, at an axial height of 350 mm, of the cylindrical cyclone at different times is shown in Fig. 8. In the simulation, the inlet velocity and the overflow split ratio were set to $3 \, \text{m s}^{-1}$ and 0.2, respectively. It was observed that the central vortex of the cylindrical cyclone rotated from the point with the lowest pressure, rather than the central point of the geometric structure, and that the position of the central vortex changed continuously with time.

In this simulation, the center point of the central vortex of the cylindrical cyclone, which is the lowest point of pressure, was marked, and the center of the central vortex structure in the unsteady flow was recorded. The results are shown in Fig. 9. The swing of the central vortex presents an approximately periodic circular motion, and the closer to the bottom of the cylindrical cyclone, the wider the fluctuation range of the pressure center.

The change in the position of the central vortex in the cylindrical cyclone leads to changes in the flow field. The pressure fluctuation amplitude and frequency in the cylindrical cyclone for different axial heights are shown in Figs. 10 and 11, respectively. Pressure detection
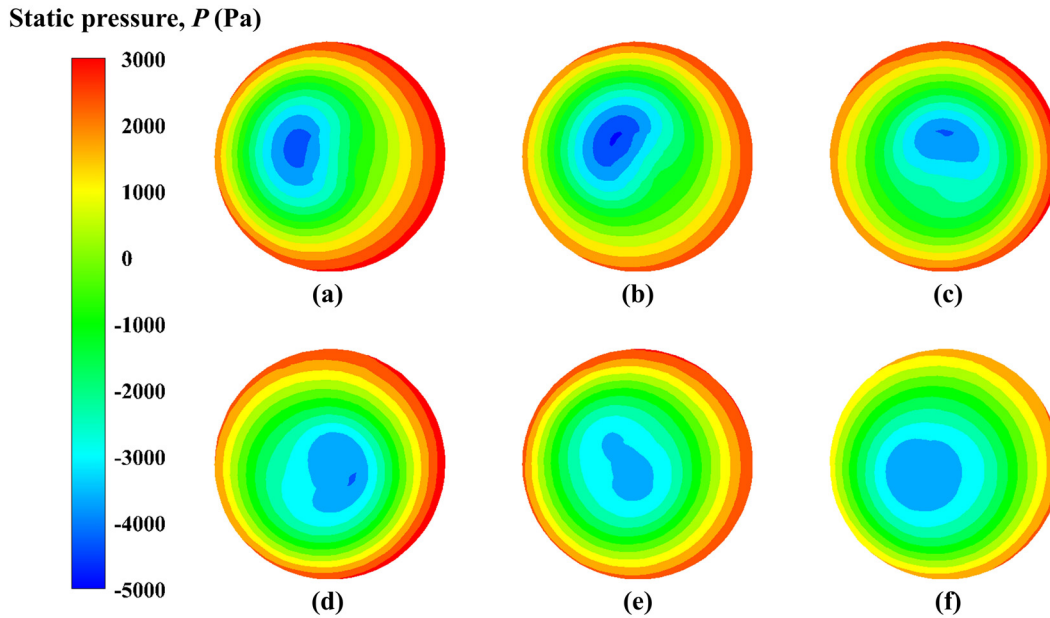
08 April 2024 03:28:50

FIG. 8. Pressure variation with time on a given cross section of the cylindrical cyclone: (a) 2.2, (b) 2.3, (c) 2.4, (d) 2.55, (e) 2.7, and (f) 2.9 s.

was carried out at selected points on the different locations of the cylindrical cyclone. The pressure fluctuation amplitude at different axial heights is shown in Fig. 10. It is observed that pressure fluctuations differ markedly. As pressure decreases with the increase in axial height,[10] the pressure fluctuations have large fluctuations near the overflow. It can also be seen that pressure fluctuations at different axial heights show periodic fluctuation. The frequency spectra of pressure fluctuations at different monitoring points are shown in Fig. 11. It is observed that the pressure fluctuation frequency at different locations is constant at a given inlet velocity and split ratio. Therefore, the

FIG. 9. Motion trajectory of central vortex.

monitoring point at the axial height of 950 mm can be used to analyze the pressure fluctuation frequency. For the inlet velocity of $3 \, \mathrm{m \, s^{-1}}$ and the split ratio of 0.2, it is approximately 25.33 Hz.

B. Effect of overflow split ratio on vibration

In this section, the influence of the ratio of flow at the two outlets of the cylindrical cyclone on the unsteady flow field is considered. A series of overflow split ratios ranging from 0.1 to 0.5 were set in the numerical simulation, all at an inlet velocity of $3 \, \mathrm{m \, s^{-1}}$. The pressure fluctuation at a given axial height for different split ratios is shown in Fig. 12. It can be seen that with the increase in split ratio, there is a stronger pressure fluctuation. The change in pressure fluctuation frequency at a given location for different split ratios is shown in Fig. 13. The pressure fluctuation frequency in the cylindrical main body shows a decreasing trend with increasing split ratio. Overall, however, this decrease is not significant. For example, when the overflow split ratio increases from 0.1 to 0.5, the pressure fluctuation frequency decreases from 26.15 to 23.15 only. Therefore, the influence of split ratio on the frequency of pressure fluctuation can be ignored. A previous research work showed that an increase in the overflow split ratio would extend the length of the central vortex,[10] which explains the reason why the frequency of pressure fluctuation decreases when the split ratio increases. In conjunction with our results (Fig. 12), a larger overflow split ratio brings more intense vibration to the cylindrical cyclone. The spectra of pressure fluctuation at different split ratios are shown in Fig. 14. By comparing the frequency profiles of the pressure fluctuation at different overflow split ratios, it is observed that increasing the overflow split ratio also makes the pressure fluctuation more complex.

V. EFFECT OF INLET VELOCITY ON VIBRATION

In this section, the influence of the inlet velocity of the cylindrical cyclone on the unsteady flow characteristics is considered. The inlet
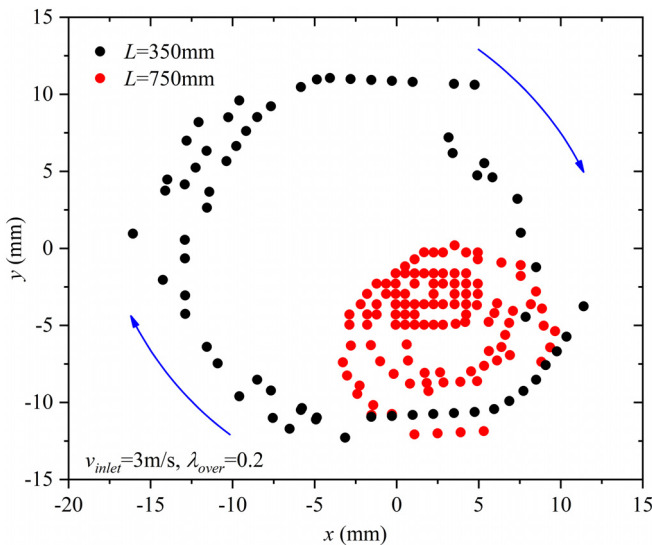
FIG. 11. Pressure fluctuation spectrum at different monitoring points.

FIG. 10. Pressure fluctuation at different axial heights.
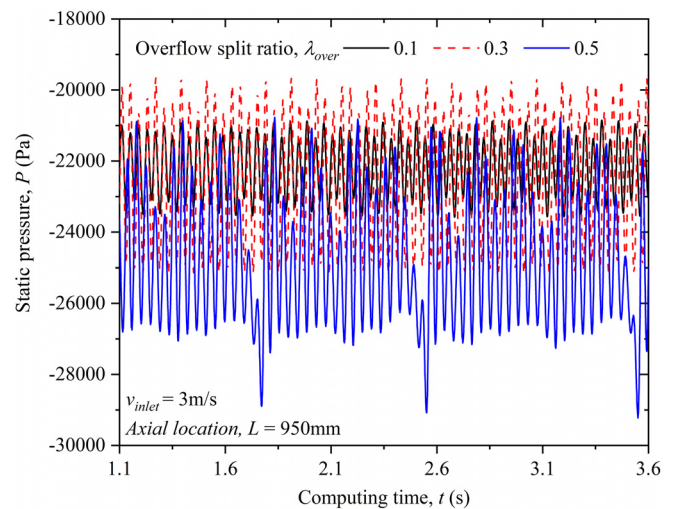
FIG. 12. Pressure fluctuation at a given point at different overflow split ratios.

velocity was varied from 2 to 5 m·s^{-1} for the numerical simulation. Pressure fluctuation spectra at different inlet velocities are shown in Fig. 15. The overflow split ratio used in the simulation was 0.2. Because the increase in inlet velocity increases the strength of the rotational flow field, it is observed that both the frequency and amplitude of pressure fluctuation increase significantly as the inlet velocity increased. Therefore, increasing the inlet velocity will increase the flow instability in the main cylinder and cause greater pressure fluctuation. The relationship between pressure fluctuation frequency and inlet velocity is shown in Fig. 16. It is concluded that the frequency of pressure fluctuation on the given 950 mm height section increases linearly with inlet velocity with a slope of 8.06 when the inlet velocity ranges from 2 to 5 m·s^{-1}.

VI. STRUCTURAL RESPONSE TO OIL–WATER TWO-PHASE FLOW-INDUCED VIBRATION

In this section, the structural vibration caused by the strong swirling motion of the mixed liquid in the process of oil–water separation
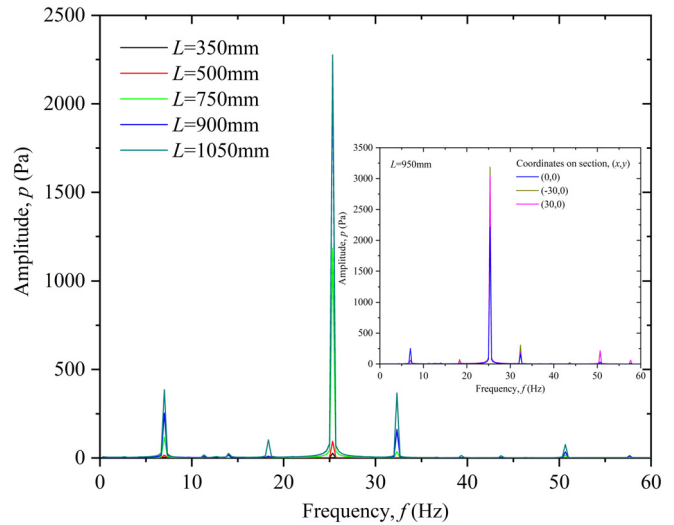
in the cylindrical cyclone is analyzed. In petroleum industry applications, the cylindrical cyclone is usually fixed on a base, operated in an upright configuration, and connected with other pipe separation instruments to form a complete oil–water mixture separation system.[12]

The vibration deformation at a given monitoring point is shown in Fig. 17. The vibration monitoring point was set to the up-outlet of the cylindrical cyclone to detect the vibration deformation of the cylindrical cyclone in three directions: x-direction (vertical to inlet), y-direction (parallel to inlet), and z-direction (vertical to base). The inlet velocity and overflow split ratio were set to 5 m·s^{-1} and 0.3, respectively. As shown in Fig. 17, the vibration deformation in all three directions shows regular changes, and under the condition of a fixed constraint at the bottom, the vibration deformation in the z-direction
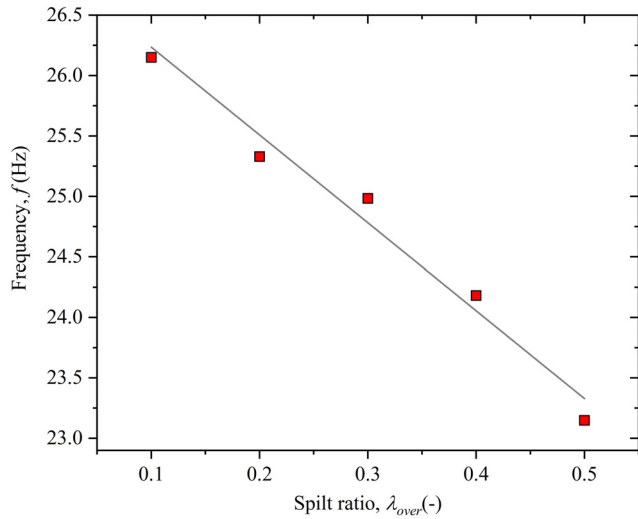
FIG. 13. Frequency of pressure fluctuation at different overflow split ratios.
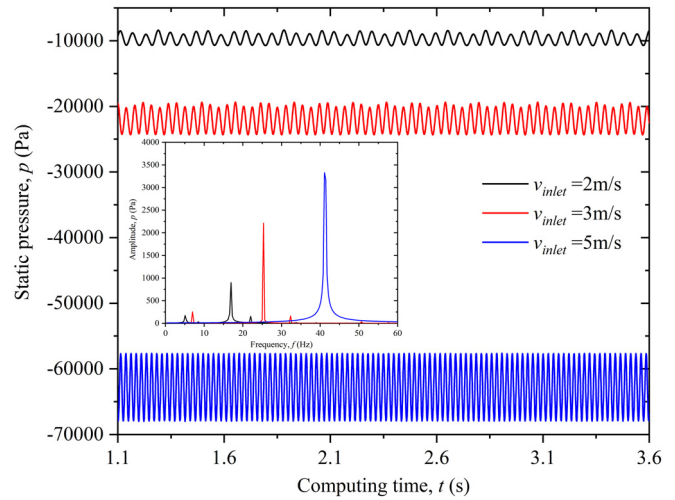

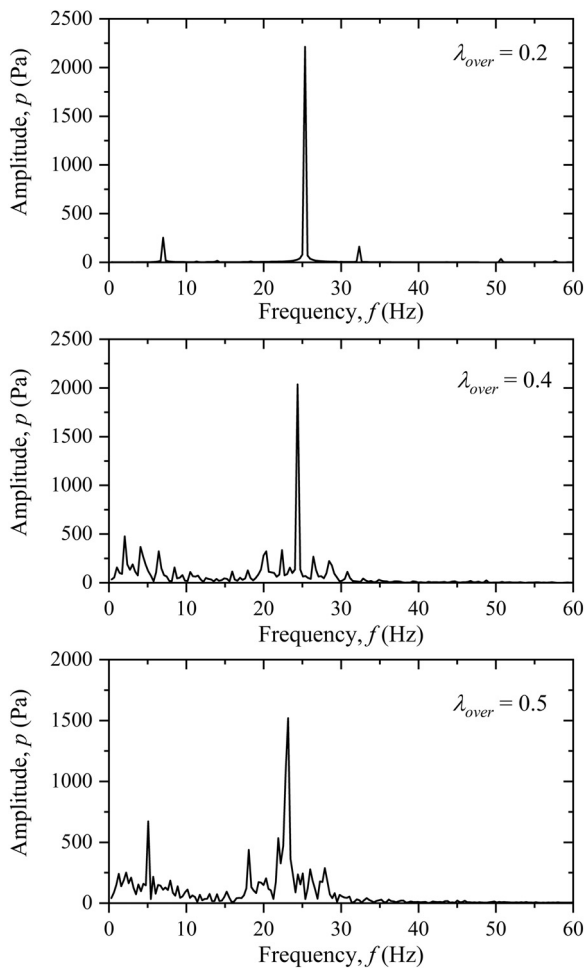FIG. 15. Pressure fluctuation at a given point at different inlet velocities.

FIG. 14. Spectrum of pressure fluctuation at different split ratios.
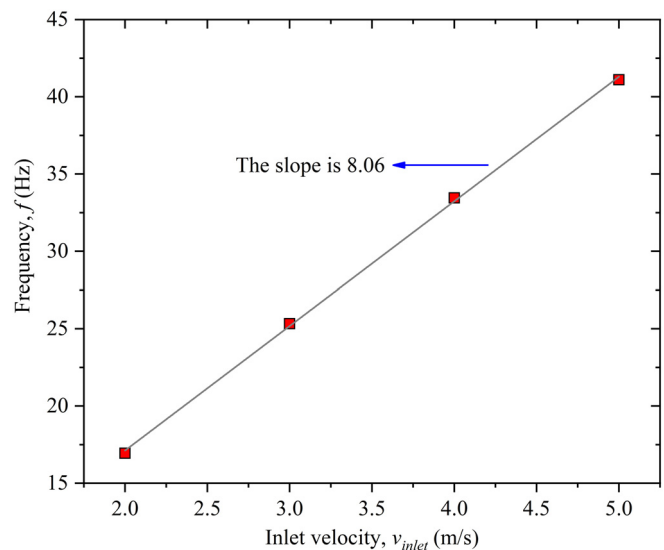

FIG. 16. Frequency of pressure fluctuation at different inlet velocities.

is the smallest, which is one order of magnitude smaller than that in the x- and y-direction. As the inflow direction is along the transverse direction, the transverse vibration deformation is the largest; the symmetric center of vibration deformation deviates along the flow direction.

The vibration displacement traces are shown in Fig. 18. Given that the vibration deformation in the z-direction is smaller than that in the other two directions, only the x- and y-directions were considered in the motion trace depicting the monitoring point. From Fig. 18, it is observed that the monitoring point data followed an approximate circular path within a parallelogram region. Comparing Figs. 9 and 18, it is observed that the motion mode of the central vortex of the cylindrical cyclone with vortex finder corresponds to the motion mode of the structure.
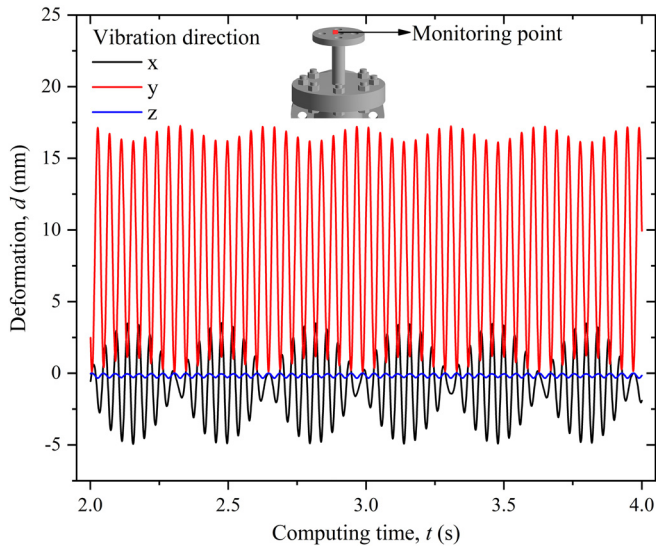
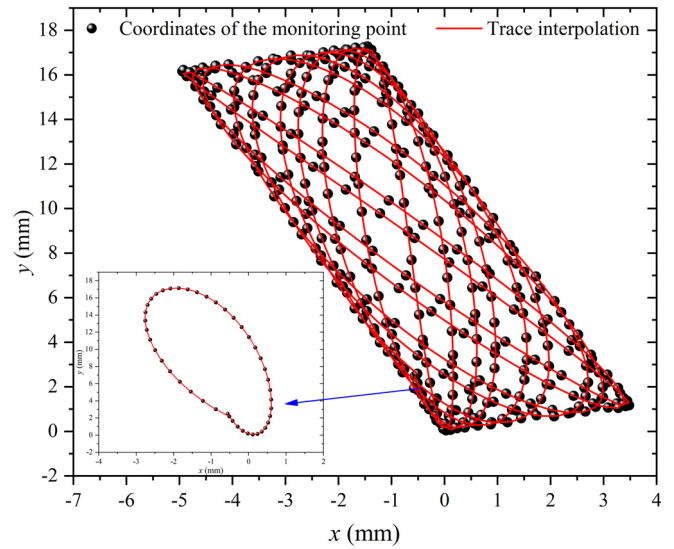**FIG. 17.** Vibration deformation at detection point.

FIG. 18. Vibration displacement traces at detection point.

The maximum equivalent stress of the cylindrical cyclone varies with inlet velocity and split ratio, which is shown in Fig. 19. It is seen that the maximum equivalent stress occurs at the connection between the underflow pipeline and the main cylinder. This is because of the moving direction of the cylindrical cyclone toward the inlet mixture,

which is affected by bottom restrictions and the shape change at the joint of the underflow pipeline and main cylindrical. Stress concentrations occur in this area; the maximum equivalent stress increases with increasing inlet velocity and split ratio. The effect of inlet velocity on equivalent stress is more significant. Therefore, the application of a
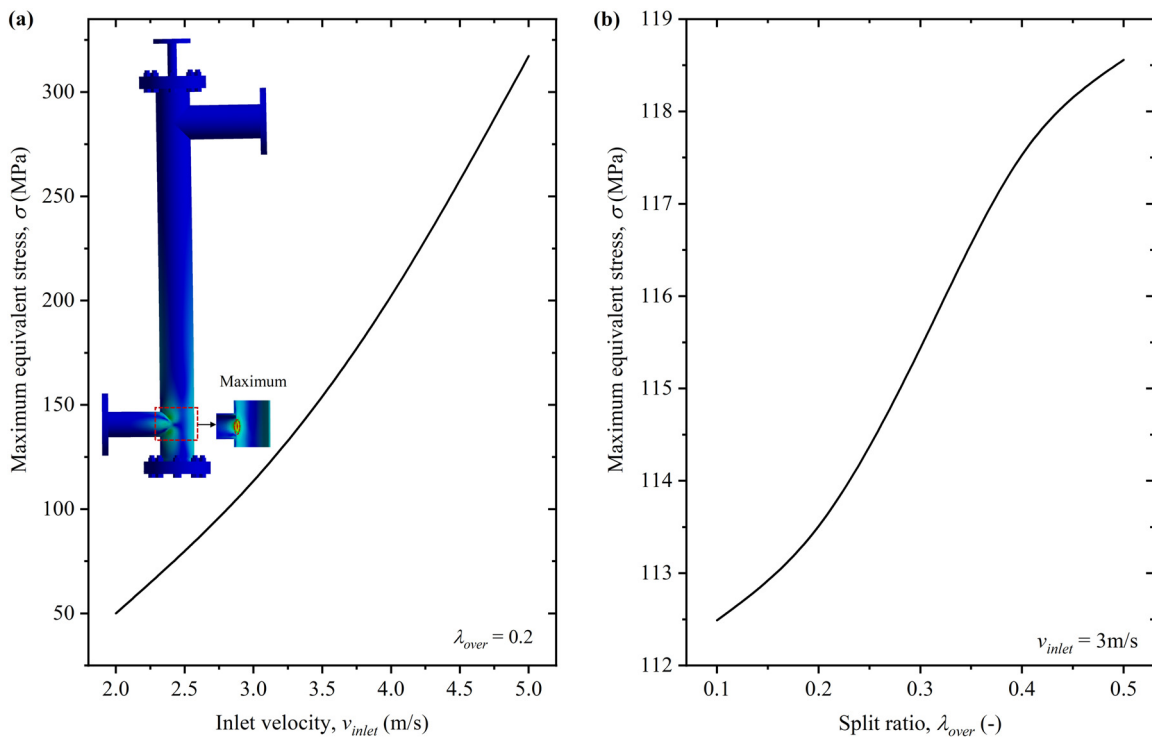

FIG. 19. Maximum equivalent stress varies with inlet velocity and split ratio: (a) inlet velocity and (b) split ratio.

TABLE IV. Physical property parameters of structural materials for the cylindrical cyclone.

Density (kg/m^3)	Young's modulus	Poisson's ratio
7850	2×10^{11}	0.3

TABLE V. First six-order frequency of the cylindrical cyclone.

Modal	Frequency (Hz)	Modal	Frequency (Hz)
First	24.71	Fourth	160.02
Second	72.21	Fifth	199.34
Third	108.92	Sixth	227.38

high inlet flow rate for separating oil–water mixture also requires higher structural strength of the cylindrical cyclone.

VII. MODAL ANALYSIS OF THE CYLINDRICAL CYCLONE

A modal analysis is needed for studying structural dynamic characteristics and for calculating natural frequencies and vibration modes.[38] The low-order modal frequency value has a major effect on whether a structure has resonance. In this section, the low-order modes of the cylindrical cyclone are analyzed. See Table IV for the material property parameters of the simulated mid-column cyclone.

In the application of cylindrical cyclones, because of the effect of damping and stiffness of the internal fluid, the influence of the fluid on the structural vibration mode and frequency needs to be considered. Therefore, a wet-mode analysis of the cylindrical cyclone is required. The first six modes for the modal analysis are shown in Fig. 20, and the first six natural frequencies are shown in Table V. It can be seen that the mode shapes of the low-order natural frequencies are mainly vibration.

Based on the analysis in Sec. IV, we know that the pressure fluctuation frequency of the unsteady flow of the cylindrical cyclone is similar to the first natural frequency. When the fluctuation frequency is close to the natural frequency, the structure can easily produce resonance phenomenon, resulting in large vibration deformations. This makes the separation of oil and water an unstable process, reduces the separation effect, and also reduces the service life of the cylindrical cyclone. Therefore, cylindrical cyclone should avoid resonance in

industrial applications. To solve this problem, an optimization scheme was proposed, imposing an additional fixed constraint on the top of the cylindrical cyclone. In this case, the corresponding first six mode shapes are shown in Fig. 21, and the corresponding frequency values of the first six orders are shown in Table VI. It can be seen that with the addition of the top constraint, the cylindrical cyclone structure can effectively avoid the resonance frequency domain.

VIII. CONCLUSIONS

The vibration characteristics induced by a two-phase flow in a cylindrical cyclone with vortex finder were researched by a dimensional analysis and multiphase-flow numerical simulation systematically. The flow characteristics of the internal flow field were analyzed to describe the distribution characteristics of the lowest point of the central-vortex pressure under unsteady flow conditions. It is important to understand the process and principle behind a two-phase flow-induced vibration. The pressure fluctuation frequency was obtained by measuring the pressure changes at selected points on the different locations of the device. The results show that the pressure in a cylindrical cyclone varies periodically during separation and that fluctuation frequency is related to the inlet velocity and flow split ratio. The effect of the flow split ratio on the pressure fluctuation frequency can be negligible, but it has a great influence on the amplitude. Therefore, the frequency of pressure fluctuation in the cylindrical cyclone with fixed structure can be obtained from the following relationship:
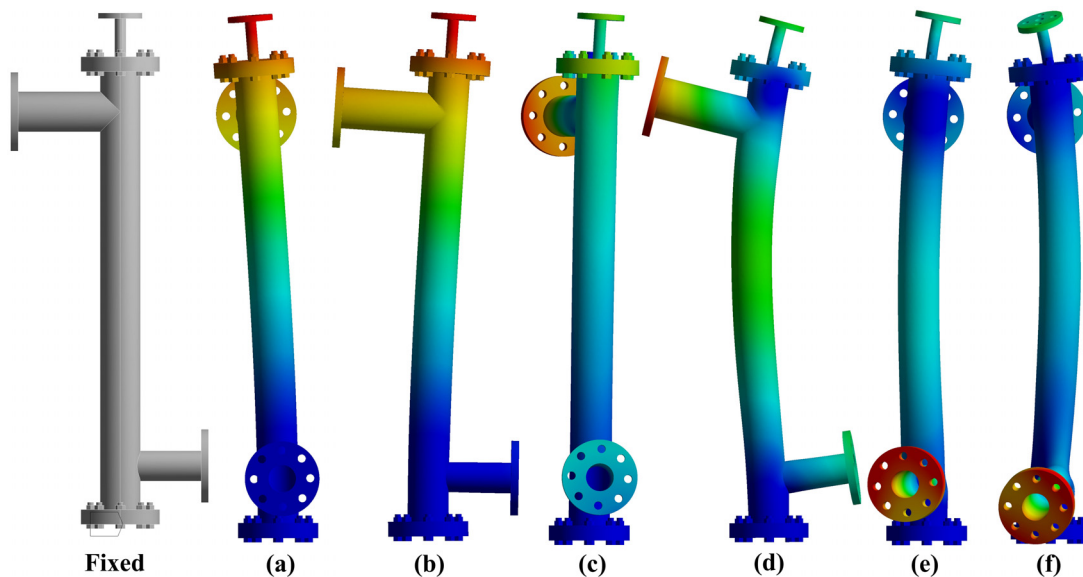

FIG. 20. Vibration pattern of the first six-order modes of the cylindrical cyclone: (a) first mode, (b) second mode, (c) third mode, (d) fourth mode, (e) fifth mode, and (f) sixth mode.
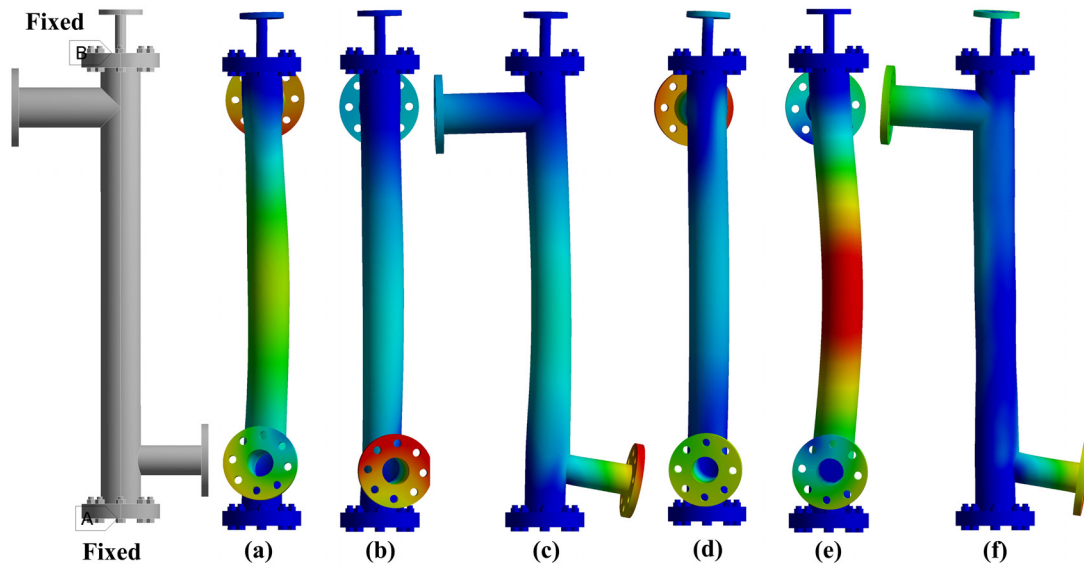
FIG. 21. Vibration pattern of the first six modes with an additional top constraint: (a) first mode, (b) second mode, (c) third mode, (d) fourth mode, (e) fifth mode, and (f) sixth mode.

TABLE VI. First six-order frequency with an additional top constraint.

Modal	Frequency (Hz)	Modal	Frequency (Hz)
First	203.09	Fourth	261.87
Second	221.63	Fifth	310.88
Third	236.56	Sixth	383.39

$$f = c \cdot \frac{v_{\text{inlet}}}{D_{\text{in}}}, \qquad (16)$$

where, for this work, the constant c is 0.806. For the cylindrical cyclone with fixed inlet, only the flow split ratio needs to be adjusted to obtain the best separation effect, but larger overflow split ratios bring more intense pressure fluctuations, which need to be understood.

The method of fluid–structure interaction for the numerical simulation was used to study the response of the cylindrical cyclone structure during the separation process. Considering the influence of different inlet velocities and flow split ratios on the structural response, the results show that the structural vibration response is consistent with the response state of the lowest point of the internal central-vortex pressure. The stress response of the structure increases with the increase in the inlet velocity and the flow split ratio, but comparing with the change in the inlet velocity, the stress change caused by the change in the flow split ratio is small. The modal analysis of the structure shows that the first-order frequency under single bottom restraint is close to the fluctuation frequency of pressure, which can easily cause resonance.

ACKNOWLEDGMENTS

AUTHOR DECLARATIONS
Conflict of Interest

The authors have no conflicts to disclose.

Author Contributions

Hu Chen: Data curation (equal); Investigation (equal); Writing – original draft (equal). **Shuo Liu:** Data curation (equal); Investigation (equal); Software (equal). **Jian Zhang:** Conceptualization (equal); Funding acquisition (equal); Writing – review & editing (equal). **Jingyu Xu:** Investigation (equal); Methodology (equal).

DATA AVAILABILITY

The data that support the findings of this study are available from the corresponding author upon reasonable request.

REFERENCES

[1] C. A. O. Araujo, C. M. Scheid, J. B. R. Loureiro, T. S. Klein, and R. A. Medronho, "Hydrocyclone for oil-water separations with high oil content: Comparison between CFD simulations and experimental data," J. Pet. Sci. Eng. **187**, 106788 (2020).

[2] R. I. Dekker, A. Deblais, B. Veltkamp, P. Veenstra, W. K. Kegel, and D. Bonn, "Creep and drainage in the fast destabilization of emulsions," Phys. Fluids **33**, 033302 (2021).

[3] C. Banerjee, K. Chaudhury, E. Cid, F. Bourgeois, S. Chakraborty, A. Majumder, and E. Climent, "Oscillation dynamics of the air-core in a hydrocyclone," Phys. Fluids **34**(9), 092106 (2022).

[4] S. Y. Noh, J. E. Heo, S. H. Woo, S. J. Kim, M. H. Ock, Y. J. Kim, and S. J. Yook, "Performance improvement of a cyclone separator using multiple subsidiary cyclones," Powder Technol. **338**, 145–152 (2018).

[5] H. P. Greenspan, "On centrifugal separation of a mixture," J. Fluid Mech. **127**, 91–101 (1983).

[6] P. Qian, J. Ma, Y. Liu, X. J. Yang, Y. H. Zhang, and H. L. Wang, "Concentration distribution of droplets in a liquid-liquid hydrocyclone and its application," Chem. Eng. Technol. **39**(5), 953–959 (2016).

[7] N. K. G. Silva, D. O. Silva, L. G. M. Vieira, and M. A. S. Barrozo, "Effect of underflow diameter and vortex finder length on the performance of a newly designed filtering hydrocyclone," Power Technol. **286**, 305–310 (2015).

[8] E. Afanador, "Oil-water separation in liquid-liquid cylindrical cyclone separator," M.S. thesis (The University of Tulsa, 1999).

[9] I. A. Dharma, F. Arffan, A. R. Prambudi, A. Widyaparaga, I. Pranoto, and Khasani, "Development of liquid-liquid cylindrical cyclone (LLCC) separator for oil-water separation," AIP Conf. Proc. **1737**(1), 040013 (2016).

[10] J. Zhang, Y. T. He, S. Liu, and J. Y. Xu, "Oil-water separation in a cylindrical cyclone with vortex finder," Phys. Fluids **34**(3), 033314 (2022).

[11] R. S. Mathiravedu, S. Wang, R. S. Mohan, O. Shoham, and J. D. Marrelli, "Performance and control of liquid–liquid cylindrical cyclone separators," J. Energy Res. Technol. **132**, 011001 (2010).

[12] H. F. Liu, J. Y. Xu, J. Zhang, H. Q. Sun, J. Zhang, and Y. X. Wu, "Oil/water separation in a liquid–liquid cylindrical cyclone," J. Hydrodyn. **24**(1), 116–123 (2012).

[13] S. Y. Shi, Y. X. Wu, J. Zhang, J. Guo, and S. J. Wang, "A study on separation performance of a vortex finder in a liquid-liquid cylindrical cyclone," J. Hydrodyn. **22**(5), 380–386 (2010).

[14] S. Miwa, M. Mori, and T. Hibiki, "Two-phase flow induced vibration in piping systems," Prog. Nucl. Energy **78**, 270–284 (2015).

[15] A. R. Kabiri-Samani, S. M. Borghei, and M. H. Saidi, "Fluctuation of air-water two-phase flow in horizontal and inclined water pipelines," J. Fluids Eng. **129**(1), 1–14 (2007).

[16] L. Ma, K. Lin, D. Fan, J. Wang, and M. S. Triantafyllou, "Flexible cylinder flow-induced vibration," Phys. Fluids **34**(1), 011302 (2022).

[17] M. J. Pettigrew, C. E. Taylor, N. J. Fisher, M. Yetisir, and B. A. W. Smith, "Flow-induced vibration: Recent findings and open questions," Nucl. Eng. Des. **185**(2–3), 249–276 (1998).

[18] T. A. Grimble and A. Agarwal, "Characterisation of acoustically linked oscillations in cyclone separators," J. Fluid Mech. **780**, 45–59 (2015).

[19] T. A. Grimble, A. Agarwal, and M. P. Juniper, "Local linear stability analysis of cyclone separators," J. Fluid Mech. **816**, 507–538 (2017).

[20] M. Ghodrat, S. B. Kuang, A. B. Yu, A. Vince, G. D. Barnett, and P. J. Barnett, "Numerical analysis of hydrocyclones with different vortex finder configurations," Miner. Eng. **63**, 125–138 (2014).

[21] H. Hu, W. Zhao, and D. Wan, "Vortex-induced vibration of a slender flexible riser with grooved and spanwise strips subject to uniform currents," Phys. Fluids **34**(12), 125131 (2022).

[22] X. Zhang, J. Wang, and D. Wan, "Euler-Lagrange study of bubble drag reduction in turbulent channel flow and boundary layer flow," Phys. Fluids **32**(2), 027101 (2020).

[23] A. Clausse and M. L. Bertodano, "Natural modes of the two-fluid model of two-phase flow," Phys. Fluids **33**, 033324 (2021).

[24] S. Balachandar, "Lagrangian and Eulerian drag models that are consistent between Euler-Lagrange and Euler–Euler (two-fluid) approaches for homogeneous systems," Phys. Rev. Fluids **5**(8), 084302 (2020).

[25] O. Elsayed, R. Kirsch, S. Osterroth, and S. Antonyuk, "An improved scheme for the interface reconstruction and curvature approximation for flow simulations of two immiscible fluids," Int. J. Multiphase Flow **144**, 103805 (2021).

[26] J. Zhang, Q. L. Wu, S. Liu, and J. Y. Xu, "Investigation of the gas-liquid two-phase flow and separation behaviors at inclined T-junction pipelines," ACS Omega **5**, 21443–21450 (2020).

[27] A. Prosperetti and G. Tryggvason, *Computational Methods for Multiphase Flow* (Cambridge University Press, 2007).

[28] J. Chen and Q. S. Li, "Nonlinear dynamics of a fluid–structure coupling model for vortex-induced vibration," Int. J. Struct. Stab. Dyn. **19**(7), 1950071 (2019).

[29] R. Messahel, C. Regan, M. H. Souli, and C. Ruiu, "Numerical investigation of homogeneous equilibrium model and fluid-structure interaction for multiphase water flows in pipes," Int. J. Multiphase Flow **98**, 56–66 (2018).

[30] J. Zhao, X. Ma, and H. Yang, "Improved modal sensitivity analysis-based method for harmonic resonance analysis," Electr. Power Syst. Res. **193**, 106978 (2021).

[31] J. A. Delgadillo and R. K. Rajamani, "A comparative study of three turbulence-closure models for the hydrocyclone problem," Int. J. Miner. Process **77**(4), 217–230 (2005).

[32] S. Heinz, R. Mokhtarpoor, and M. Stoellinger, "Theory-based Reynolds-averaged Navier-Stokes equations with large eddy simulation capability for separated turbulent flow simulation," Phys. Fluids **32**, 065102 (2020).

[33] G. Sharma and J. Majdalani, "Effects of nozzle inlet size and curvature on the flow development in a bidirectional vortex chamber," Phys. Fluids **33**(9), 093607 (2021).

[34] F. Hamba, "History effect on the Reynolds stress in turbulent swirling flow," Phys. Fluids **29**(2), 025103 (2017).

[35] A. Escue and J. Cui, "Comparison of turbulence models in simulating swirling pipe flows," Appl. Math. Modell. **34**(10), 2840–2849 (2010).

[36] B. Yang and Z. Yang, "On the wavenumber-frequency spectrum of the wall pressure fluctuations in turbulent channel flow," J. Fluid Mech. **937**, A39 (2022).

[37] C. Vezyris, E. Papoutsis-Kiachagias, and K. Giannakoglou, "On the incremental singular value decomposition method to support unsteady adjoint-based optimization," Int. J. Numer. Methods Fluids **91**(7), 315–331 (2019).

[38] P. Weis, L. Kucera, P. Pechac, and M. Mocilan, "Modal analysis of gearbox housing with applied load," Procedia Eng. **192**, 953–958 (2017).

08 April 2024 03:28:50